Electrochemistry Communications 179 (2025) 108011

Contents lists available at ScienceDirect

Electrochemistry Communications

journal homepage: www.elsevier.com/locate/elecom

The impact of metallic impurities on the activity-stability relationship of iridium-based nanofiber catalysts for acidic water electrolysis

Miklós Márton Kovács [a,b], Karl J.J. Mayrhofer [a,b], Dominik Dworschak [a,*]

[a] Forschungszentrum Jülich GmbH, Helmholtz Institute Erlangen-Nürnberg for Renewable Energy (IET-2), 91058 Erlangen, Germany
[b] Friedrich-Alexander-Universität Erlangen-Nürnberg, Department of Chemical and Biological Engineering, 91058 Erlangen, Germany

ARTICLE INFO

Keywords:
Acidic water electrolysis
Electrospinning
Fe^{3+}
Al^{3+}
OER
Dissolution

ABSTRACT

PEM water electrolyzers are operated with deionized or highly purified water. However, metallic impurities can appear in the pipes as well as in the inner compartment due to corrosion of the metal parts of the electrolyzer cell as the bipolar plate (BPP) or the porous transport layer (PTL). The dissolved ions from the cell components have an influence on the degradation and may impact the catalyst activity. Our objective is to shed light on these processes in the case of two selected metal ion contaminations, which helps us understand the relevance of selecting proper catalyst materials for acidic water splitting. In this study, the impact of cationic impurities on the electrocatalytic activity and stability of IrO_x based nanofiber catalyst materials for acidic water electrolysis is investigated in a scanning flow cell coupled with an inductively coupled plasma mass spectrometer (SFC-ICP-MS). IrO_x catalyst materials are tested in an aqueous model system of 0.1 M $HClO_4$ containing 5 ppm (molar ratio) Fe^{3+} and Al^{3+}. The reference IrO_x Alfa Aesar (AA) shows a significant increase in oxygen evolution reaction (OER) activity, while IrO_x calcined at 400 °C suffers from an activity decline of more than 50% if 5 ppm Fe^{3+} are in the electrolyte. Due to their high iridium oxide content, IrO_x species calcined at 600 °C and 800 °C exhibit no significant change regardless of the contaminant ion introduced. In terms of the stability number (S-number), the dissolution rate of the 400 °C species can be mitigated by Fe^{3+} ions, while it influenced the other catalysts only modestly. This is mainly the case for Al^{3+} ions, although a slight enhancement can be observed for the highly oxidized species of 600 °C and 800 °C. In general, the presence of Fe^{3+} and Al^{3+} ions has a controversial influence on the OER activity and the degradation of iridium-based catalyst materials, which is mainly driven by their oxidation state.

1. Introduction

Hydrogen produced via water electrolysis plays a pivotal role in the long-term storage of electricity from renewable sources. Proton exchange membrane (PEM) electrolysis is a key technology in this regard due to its ability of operating with intermittent power sources, e.g. wind and solar. The soul of an electrolysis cell is the membrane-electrode assembly (MEA), which consists of an anode (mainly IrO_2), a cathode (predominantly Pt-based) and the ion-conductive membrane between them. Several studies have been conducted on MEAs to optimize operational conditions such as current density, operating pressure, and temperature [1–3]. However, another important factor is the quality of the water. Impurities like metal ions can originate either from the feed water or the degraded components of the electrolyzer cell during operation.

Various metal ions have been reported to pose a detrimental effect on cell performance and durability [4–6]. Fe and Ni were found in the proton exchange membrane after *ex situ* tests for 2 h at +2.0 V *vs.* NHE stemming from the bipolar plates (BPPs) made of coated stainless steel (SS) [7]. SS is frequently investigated to replace Ti due to its low cost and ease of formability [8]. Fiedler et al. found that SS continued to dissolve even if the accumulation was inhibited by using an ion exchanger and high flow rates because no stable passivation layer was formed [9]. Therefore, corrosion protection coatings are recommended to mitigate metal dissolution and thus accelerated degradation of the electrolysis cell [7,10,11]. The other source of metal contamination is feed water. Li et al. observed a severe cell performance decay with already 1 ppm Fe^{3+} contamination at 0.5 A cm^{-2} and 60 °C in a long-term experiment of more than 700 h. [12], although they were able to mitigate this phenomenon at an elevated temperature of 80 °C and low current density. They could even enhance the cell performance at a higher current density of 2 A cm^{-2} and 10 ppm Fe^{3+} concentration when the operation temperature was increased from 60 °C to 80 °C due to

* Corresponding author.
E-mail address: d.dworschak@fz-juelich.de (D. Dworschak).

https://doi.org/10.1016/j.elecom.2025.108011
Received 21 February 2025; Received in revised form 15 July 2025; Accepted 22 July 2025
Available online 5 August 2025

charge and mass transport recovery [13]. Nevertheless, Fe^{3+} ions can accumulate on the anode catalyst layer, occupying active sites of the catalyst and poisoning the electrocatalyst [14]. This leads to the loss of catalytically active area and decrease of the OER reaction kinetics. Later, this research group also investigated other cationic impurities, including Al^{3+}. They found that 5 ppm Al^{3+} can even cause a sudden cell failure when introduced into the cell [15].

On the other side, research has been conducted on aluminum as an intrinsic part of the catalyst with a boosting effect on OER activity [16]. It has also been reported that the iridium content could be greatly reduced by inserting aluminum into the anodic catalyst layer of PEM water electrolyzers [17]. Lee et al. synthesized and tested Al-doped $RuIrO_x$ mixed metal oxides for the application of PEMWE successfully achieving a high current density over 4.1 A cm^{-2} and a mass activity of 3.55 A mg_{Ru+Ir}^{-1} with negligible performance degradation at 1.0 A cm^{-2} for 60 h [18]. According to the study, Al is responsible for improving the OER performance, whereas a small amount of intrinsic iridium is desirable to improve the acidic stability of the catalyst.

As for the stability of IrO_x based catalysts, it has been reported that they undergo dissolution at approximately 1.8 V in a PEM electrolyzer cell and at even lower potentials in a half-cell setup, e.g. scanning flow cell (SFC) [19,20]. Although IrO_x materials, especially the completely rutile IrO_2 is a stable anode catalyst material, the continuous O_2 gas evolution and the high overpotential caused by cation impurities at the active sites can lead to an enlarged dissolution of IrO_2 [19,21].

In this study, we investigate the impact of Fe^{3+} and Al^{3+} ions in the electrolyte on the OER activity and the dissolution behavior of selected iridium based nanofibrous catalyst materials in an accelerated and easy manner by SFC-ICP-MS. These cations were chosen because they can be present in the electrolyzer system from the stack component materials or due to corrosion of the pipes [6,19,22] .

2. Experimental section

Materials. Iridium oxide (IrO_x Premion™ Alfa Aesar 99.99%, Ir 84.5% min.) and perchloric acid ($HClO_4$ Ultrex™, 70 wt%) were purchased from Thermo Fisher Scientific. Iron(III) nitrate ($Fe(NO_3)_3 \cdot 9\ H_2O$, Emsure®) was obtained from Merck. Aluminum nitrate ($Al(NO_3)_3 \cdot 9\ H_2O$, ≥ 98%), isopropyl alcohol (IPA Emsure®, ≥ 99.8%), acetone (ACN Emsure®, ≥ 99.8%), and Nafion™ (1100 W dispersion, 5 wt%) were purchased from Sigma Aldrich. Glassy carbon plates (GC, 5 x 5 cm^2, HTW Sigradur G) were supplied by HTW. Potassium hydroxide (KOH, 99.98%) and nitric acid (HNO_3 ROTIPURAN® Ultra, 69 wt%) were obtained from Carl Roth. Deionized water (Millipore, 18.2 MΩ cm at 25 °C, TOC < 3 ppb) was used to prepare the aqueous solutions.

Nanofiber synthesis. The synthesis of the nanofibrous catalyst materials has been published elsewhere, along with material characterization [23]. In short, the precursor solution of $IrCl_3 \cdot x\ H_2O$, poly(vinylpyrrolidone) (PVP) and DI water was electrospun at 20 kV. The nanofibers (NFs) were collected on a rotating drum collector covered with an aluminum foil. After electrospinning, calcination took place under synthetic air atmosphere at various temperatures to create the final catalyst in the form of IrO_x.

Ink preparation. The detailed description of the ink preparation and the drop-casting process on the GC substrate can be found in our previous study [23].

Electrochemical and stability measurements (SFC-ICP-MS). All samples are tested in a scanning flow cell (SFC) coupled with ICP-MS described elsewhere [24]. The electrolyte is pumped through the V-shaped channels of a polycarbonate SFC. On the bottom side, the SFC has an elliptical opening of 0.036 cm^2. The electrolyte has a hanging meniscus which establishes the ionic contact between the drop-cast IrO_x spots operating as the working electrode (WE) and the reference (RE, Hydroflex Mini, Gaskatel) as well as the counter electrode (CE, GC rod, d = 1.6 mm, HTW Sigradur G). Both electrodes are placed in a separate compartment in stagnant electrolyte. The concentration of the analyte and the internal standard (ISTD) isotopes are constantly detected, and the analyte signal is normalized by the ISTD intensity. The calibration is conducted by a five-point measurement including the blank and the concentrations of 0.5, 2, 5, and 10 ppb. We use 3 μg l^{-1} of ^{187}Re, 10 μg l^{-1} of ^{45}Sc, and 50 μg l^{-1} of ^{72}Ge as ISTD to monitor ^{193}Ir, ^{27}Al, and ^{56}Fe, respectively.

5 ppm (molar ratio) Al^{3+} and Fe^{3+} solutions are prepared with 0.1 M $HClO_4$ as the background electrolyte. As for Fe^{3+}, setting a strong acidic pH was crucial to prevent its hydrolysis. We assume a constant ion concentration neglecting the amount of ions adsorbed on the electrode surface and the tubings, which proved plausible as the test protocol conducted was short. The details of the test protocol are described in our previous study [23]. Shortly, after the open-circuit potential (OCP), linear sweep voltammetry (LSV) was used to determine the OER activity of the catalyst materials. Afterwards, a chronopotentiometric hold was recorded to model the OER at a constant current density (1 mA cm^{-2}) and calculate a comparable S-number as the figure of merit for dissolution rate and OER activity [25]. Finally, potentiostatic electrochemical impedance spectroscopy (PEIS) was applied to identify the ohmic resistance of the electrolyte.

3. Results and discussion

A summary of the dissolution of all species can be found in Fig. 1 conducted by SFC-ICP-MS, where the on-line dissolution rates are detected during the electrochemical protocol applied (top axis). The most pronounced difference between the presence of Al^{3+} and Fe^{3+} can be observed in the case of IrO_x calcined at 400 °C. Namely, the dissolution of this species can easily be followed in Fig. 1a, and clear dissolution peaks can be ascribed to the individual steps of the electrochemical protocol applied. For IrO_x calcined at 600 °C and 800 °C as well as the reference IrO_x AA, less Ir dissolves than for IrO_x 400. However, both peaks induced by the LSV step and contacting the catalyst spot with the electrolyte can be identified easily. Nevertheless, this changes considerably when Fe^{3+} ions are present in the electrolyte (Fig. 1b) instead of Al^{3+}: the change in the dissolution behavior is the most conspicuous in the case of IrO_x 400.

To find out the reason for this phenomenon, we consider the S-number for the comparison of the dissolution behavior of distinct IrO_x species as the key figure of merit. For Al^{3+} ions present in the electrolyte, we observe a modest increase for all catalyst materials tested but the reference (Fig. 2a). However, by the addition of Fe^{3+}, IrO_x AA and 600 undergo no change, whereas the stability of IrO_x 400 can be improved slightly more. IrO_x calcined at 800 °C shows an insignificant change in the stability, though, independent from the metal ion at the certain concentration investigated. The dissolution rates of each catalyst material investigated are shown in Figure S2-S5 of the Supplementary Information (SI) for each electrolyte composition.

Regarding IrO_x 400, the enhanced stability can have two reasons based on the definition of the S-number: A) an enhanced OER activity resulting in more O_2 produced, or B) making the catalyst surface more stable resulting in less Ir dissolved [25].

In case A, we consider the OER activity of the catalyst materials aforementioned. In Fig. 2b, the mass-specific activity (*MA*) of selected IrO_x-based nanofiber catalyst materials (calcined at 400 °C, 600 °C, and 800 °C) as well as the reference IrO_x AA is depicted.

Aluminum and iron(III) ions lead to no significant increase in the OER activity of IrO_x AA compared their absence (817.0 ± 357.0 and 555.5 ± 25.9 A g_{Ir}^{-1} for Al^{3+} and Fe^{3+}, respectively, compared to 497.5 ± 314.6 A g_{Ir}^{-1} with no impurities), although considerable deviations are observed. 5 ppm Al^{3+} results in an approx. 28% lower *MA* of IrO_x calcined at 400 °C, while 5 ppm Fe^{3+} exhibits a detrimental effect (−51%). As for IrO_x calcined at 600 °C, Al^{3+} and Fe^{3+} do not cause a notable improvement in OER activity as in the case of the reference. Likewise, the catalyst IrO_x calcined at 800 °C of complete

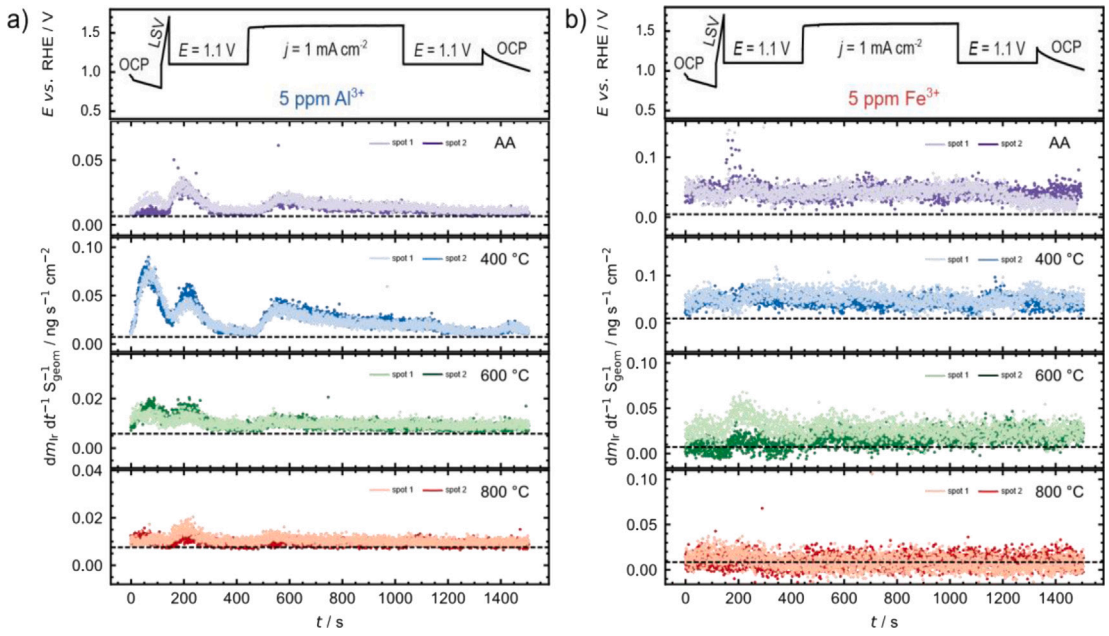

Fig. 1. (a) Dissolution rates of all species investigated in the presence of 5 ppm Al^{3+} throughout the entire electrochemical protocol. (b) Dissolution rates of all species investigated in the presence of 5 ppm Fe^{3+}. The detection limit (DL) is given for every catalyst material as dashed line, and is defined as $c_{DL} = 3s_{blank}/m$, where s_{blank} and m is the standard deviation of the background signal and the slope of the calibration curve, respectively.

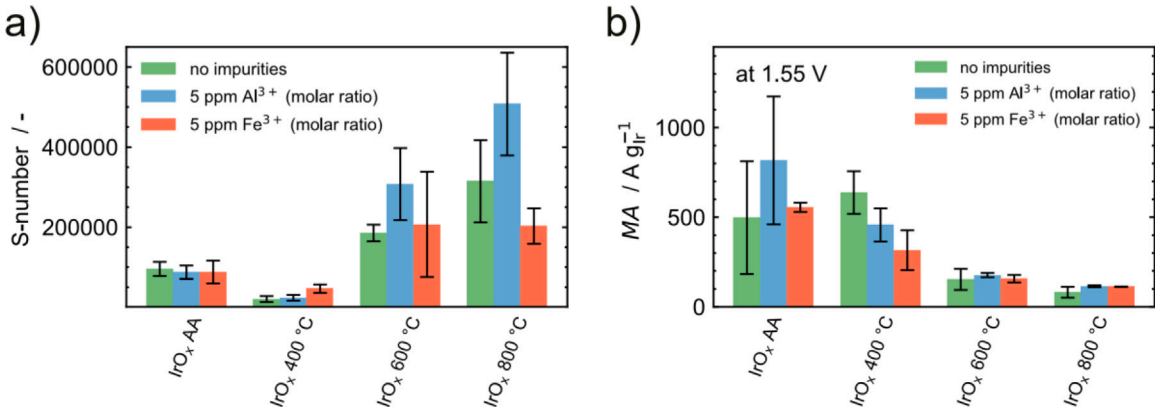

Fig. 2. (a) Mass activity of the four catalyst materials investigated at 1.55 V *vs.* RHE in 0.1 M $HClO_4$, with 5 ppm Al^{3+}, and 5 ppm Fe^{3+} as impurities in the electrolyte flow. The current density is normalized to the iridium loading of the catalyst spots (10 μ g_{Ir} cm^{-2}). (b) Stability number of IrO_x nanofibrous catalyst materials calcined at 400 °C, 600 °C, and 800 °C, as well as the reference material IrO_x Alfa Aesar. The comparison is made with no impurities (pure background electrolyte of 0.1 M $HClO_4$), 5 ppm Al^{3+}, and 5 ppm Fe^{3+}.

rutile structure experiences no significant deterioration against metallic impurities in the electrolyte which is in accordance with previous results [26].

Nevertheless, we summarize all geometric current density values (j_{geo}), mass-specific (*MA*) and area-specific (*SA*) activities in Table S1 of the Supplementary Information (SI) obtained at various potentials. Moreover, j_{geo} and *SA* values at 1.55 V *vs.* RHE are highlighted in Figure S1. We observe that the current density detected increases in smaller steps for Al^{3+} and Fe^{3+} with increasing potential during the LSV measurement. We find IrO_x calcined at 600 °C and 800 °C are indeed stable against degradation by Al^{3+} and Fe^{3+} impurities. We believe, this behavior originates from its nearly (600 °C) and completely (800 ° C) rutile structure [23]. As for IrO_x calcined at 400 °C, we ascribe this phenomenon to its high proportion of metallic Ir, which is more prone to catalyst poisoning than its oxide counterparts [27]. The same trends can be seen for j_{geo} and *SA* in Table S1.

After we discussed the detrimental effect of Fe^{3+} ions in the electrolyte on the OER activity of IrO_x calcined at 400 °C in Fig. 2b, it has become obvious that case A is not supported by experimental data. Instead, this must be the result of less Ir dissolved during the test which results in a higher S-number based on its definition (case B) [25]. This is also supported by Fig. 3a, in which the absolute amount of dissolved Ir is depicted throughout the electrochemical protocol. As demonstrated by the example of the chronopotentiometric step ('1 mA cm^{-2}') of IrO_x 400 °C, a substantial reduction of the dissolved amount of Ir can be observed (ca. 58% and 64% lower for 5 ppm Al^{3+} and Fe^{3+}, respectively, compared to the case 'no impurities'). A similar trend is shown for IrO_x AA (ca. 55% lower mass dissolution for both types of impurities compared to those without impurities), although this behavior originates from an enhanced OER activity highlighted in Fig. 2b, and clearly is not in correlation with the alteration of the dissolution mechanism based on the findings of Fig. 2a.

The reason for the enhanced stability of IrO_x calcined at 400 °C in the presence of Fe^{3+} ions is a change in the dissolution kinetics. As visible in Fig. 3b, the electrochemical potential during the galvanostatic OER step approaches 1.60 V *vs.* RHE (from 1.52 ± 0.01 to 1.57 ± 0.02 V *vs.* RHE), above which the second dissolution route becomes more prononunced leading to the formation of Ir^{VI} and the

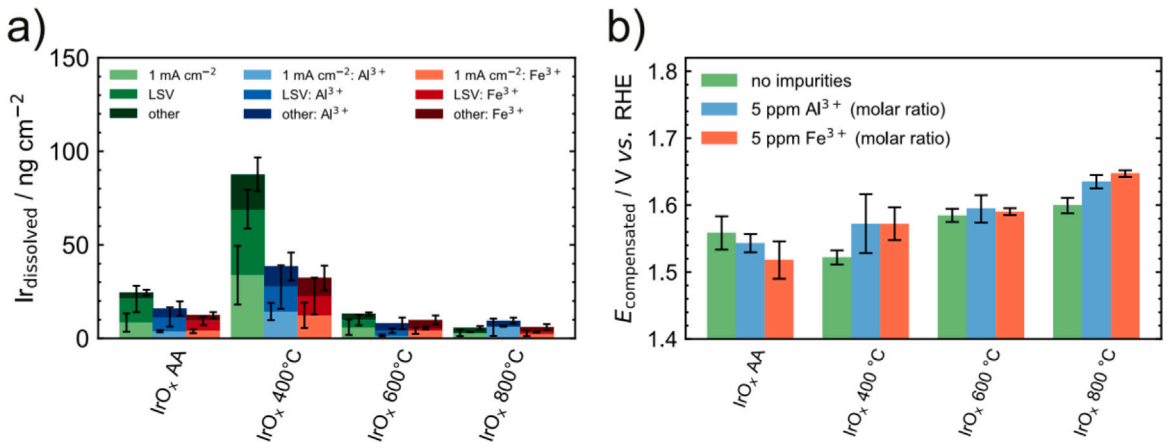

Fig. 3. (a) Stacked mass dissolution of atomic iridium calculated for the chronopotentiometric ("1 mA cm^{-2}") and the linear sweep voltammetry ("LSV") step of the electrochemical protocol applied in this study. All other steps were quantified as "other" including the contact peak at the beginning of the protocol. The dissolution is normalized to the geometric surface area of the catalyst spots. (b) Potential (iR corrected) obtained during the galvanostatic hold of 1 mA cm^{-2} of IrO$_x$ NFs after calcination at T = 400 °C, 600 °C, and 800 °C as well as the reference material in 0.1 M $HClO_4$, in the presence of 5 ppm Al^{3+}, and 5 ppm Fe^{3+}. The duration of the galvanostatic step is 600 s.

dissolution of IrO_3 and anionic Ir species as discussed in the paper of our research group previously [28]. The formation of IrO_3 and IrO_4^{2-} is kinetically slower than the formation of Ir^{3+} resulting in lower dissolution rates (in ng_{Ir} cm^{-2} s^{-1}). We have to note that we observe no similar behavior for IrO$_x$ calcined at 600 °C and 800 °C when Al^{3+} or Fe^{3+} are supplied in the electrolyte. Their potential in pure 0.1 M $HClO_4$ is already higher and is partly in the range where Ir is dissolved by the formation of IrO_4^{2-} ions. These dissolution mechanisms of Kasian et al. have universal character and can be applicable for various Ir-based oxide catalyst materials such as the nanofibers applied in this study [28].

These findings are of particularly important in the context of IrO$_x$ 400, for which metal contaminations do have a clear detrimental effect on activity. We assume that it originates from the major metallic Ir component of this sample. In general, oxide-based electrodes are not as sensitive to poisoning by the metallic impurities as pristine metal electrodes, although they exhibit a moderate electrocatalytic activity for gas evolution [27]. In the case of iridium oxide species, however, the scientific community assigns these phenomena mainly to membrane degradation [12,13,15] and Fe deposition on the anode side gasket and porous transport layer (PTL) [29], which is beyond the scope of this study. Here, we can explicitly investigate the isolated effect of these metallic impurities on the active catalyst material only to understand the possible deterioration influence.

In total, the activity-stability relationship of IrO$_x$ calcined at 400 °C and 600 °C exhibits major differences when Fe^{3+} ions are introduced into the electrolyte. Thus, it is also relevant how much Fe^{3+} causes the phenomenon of deterioration of OER activity.

To further study the influence of impurity on the catalyst, we show the impact of Fe^{3+} ions on the activity and stability at different concentrations in Fig. 4. We observe a gradual decrease in the mass-specific activity (MA) with increasing Fe^{3+} concentration for IrO$_x$ calcined at 400 °C (Fig. 4a). A significant decline can be experienced in the presence of more than 50 ppb Fe^{3+} compared to having no impurities. As for IrO$_x$ calcined at 600 °C, a rapid enhancement of the OER activity is found at low Fe^{3+} concentrations (from 134.4 ± 21.1 up to a maximum of 326.1 ± 9.8 A g_{Ir}^{-1} at 5 ppb Fe^{3+}) but a comparable MA level can be determined in the presence of 5 ppm Fe^{3+}. We believe that a small amount of Fe^{3+} contamination can improve the electrocatalytic activity of this catalyst. Increasing the Fe^{3+} concentration up to 5 ppm leads to more adsorbed species on the catalyst active centers resulting in the decrease of the electrocatalytic activity but it is still higher (143%, 122%, 128%, and 17% higher for 5 ppb, 50 ppb, 500 ppb, and 5 ppm, respectively) than with no impurities (134.4 ± 21.1 A g_{Ir}^{-1}).

As for the stability number, an increasing trend can be observed from 5 ppb to 5 ppm (−65%, -61%, +7%, and +84% difference compared to the case of no impurities for 5 ppb, 50 ppb, 500 ppb, and 5 ppm, respectively) for IrO$_x$ 400. Thus, we find the S-number at 500 ppb Fe^{3+} being in the same range with no Fe^{3+} present in the electrolyte. The latter may demonstrate the critical concentration, at which the dissolution kinetics change from positively charged Ir species to more negatively charged IrO_4^{2-} ions indicating the increase in the potential as discussed before. Regarding IrO$_x$ calcined at 600 °C, we observe only a slight alteration in the dissolution behavior due to the more oxidized — i.e. more stable — composition of the nanofiber surface (+30%, +25%, +0%, and +12% for 5 ppb, 50 ppb, 500 ppb, and 5 ppm, respectively) [23]. The dissolution rates of IrO$_x$ 400 and IrO$_x$ 600 are summarized in Figure S6 and S7 for each Fe^{3+} concentration, respectively.

We have to note that other cation impurities have also been reported with adverse effect on the performance and/or stability of electrolyzer cells. A good overview has been provided by Becker et al. [26]. One of the sources of cation impurities is feed water. Common impurities include Fe^{3+}, Mg^{2+}, Ca^{2+}, Cu^{2+}, and Na^{+} [3,6,12–15,30–33]. Mg^{2+}, Ca^{2+}, and Na^{+}, stemming from seawater or potable water, have shown a severe impact on the membrane lowering its conductivity [31,32,34–36] as well as the catalyst degradation on both electrodes [12,37–39]. On the anode, they lower the ionomer conductivity, and act as catalyst poisons [37].

Another source of cationic impurities is the cell components releasing Ti^{2+}, Ni^{2+}, and Cu^{2+} during operation. These cations have been found to accumulate on the surface of the cathode catalyst layer [40] or absorb in the membrane [5,41] However, their detrimental effect could be mitigated by implementing an ion-exchange resin and maintaining a low pH. All in all, focusing on OER catalysts, contaminants of internal sources are challenging to trace, and their impact on the catalyst activity and stability is extremely difficult to monitor in full cells at such low concentrations. Regarding external sources, especially feed water, only Na^{+} and alkaline earth metals, such as Ca^{2+} and Mg^{2+} have been found to pose a detrimental effect on OER activity and stability of the catalyst material, which could be made easily reversible when soft water was replaced with ultrapure water again during operation [42].

In conclusion, we could investigate the impact of Al^{3+} and Fe^{3+} contaminants on both the OER activity and dissolution behavior of various Ir based nanofibrous catalyst materials in an SFC-ICP-MS setup. We could directly observe the influence of the metal impurities on the catalyst material which is challenging to discuss in a full cell, where the performance losses are mainly ascribed to membrane degradation [3,12,15,27,30]. We used nitrate salts (NO_3^{-}) because no adverse effects

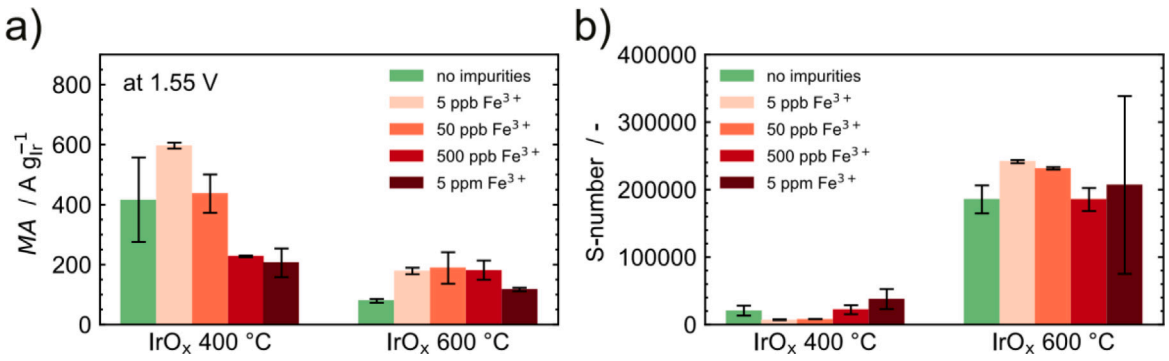

Fig. 4. (a) Mass-specific activity at 1.55 V *vs.* RHE and (b) stability number of IrO_x nanofibrous catalyst materials calcined at 400 °C, and 600 °C at different Fe^{3+} concentrations of 5 ppb, 50 ppb, 500 ppb, and 5 ppm (molar ratio). The comparison is made with no impurities (pure background electrolyte of 0.1 M $HClO_4$). The experiments were repeated at least once at each concentration.

of nitrate have been published being a catalyst poison or accelerating catalyst dissolution in contrast with Cl^- or SO_4^{-2} [43,44]. The core findings of our study revealed that:

- A high amount of 5 ppm Al^{3+} ions in the electrolyte has no significant effect on the OER activity of IrO_x based catalyst materials when their oxidation state was sufficiently high (IrO_x AA, IrO_x 600 and IrO_x 800. Similarly, Fe contamination of the same concentration (molar ratio) show no significant influence on their OER activity.
- The more metallic the catalyst surfaces the more prone to catalyst poisoning, which we could observe and confirm in the case of IrO_x calcined at 400 °C in terms of OER activity.
- An enhanced stability of IrO_x 400 was shown assuming a change in the dissolution kinetics based on an increased OER potential when Fe^{3+} ions were present.
- Furthermore, the latter phenomenon depended on the concentration of Fe impurities in the case of IrO_x 400 claiming 500 ppm to be a critical level where a significant decrease of OER activity (from 416.1 ± 140.8 A g_{Ir}^{-1} down to 227.4 ± 2.7$_{Ir}^{-1}$) and an improved S-number begins to dominate. However, this was not confirmed for IrO_x calcined at 600 °C, which performed better in terms of OER activity, regardless of the level of Fe contamination; however, it highlights no significant change in the dissolution rate.

Finally, it is desirable to know the adsorption kinetics of Al^{3+} and Fe^{3+} species on these various surfaces to find out if a mainly metallic Ir surface is more prone to the adsorption of metal impurities occupying its active centers and thus resulting in a significant loss in performance and stability, as well. If it is the case, it is of utmost priority to emphasize the relevance of the choice of the right catalyst materials, considering their morphology and composition from the very beginning.

CRediT authorship contribution statement

Miklós Márton Kovács: Writing – review & editing, Writing – original draft, Visualization, Validation, Methodology, Investigation, Formal analysis, Data curation, Conceptualization. **Karl J.J. Mayrhofer:** Writing – review & editing, Supervision, Resources, Funding acquisition. **Dominik Dworschak:** Writing – review & editing, Supervision, Project administration, Formal analysis, Conceptualization.

Declaration of competing interest

The authors declare that they have no known competing financial interests or personal relationships that could have appeared to influence the work reported in this paper.

Acknowledgments

M. M. Kovács and D. Dworschak thank the German Federal Ministry of Education and Research (BMBF) for the financial support of the HyThroughGen project (03HY108A). M. M. Kovács is grateful for the support of Nico C. Röttcher in the field of database management and data visualization. M. M. Kovács also thanks Jonas Möller for the development of the LabVIEW environment for data acquisition, and Lena Fiedler for the discussions about the importance of metallic impurities in water electrolyzer systems.

Appendix A. Supplementary data

Supplementary material related to this article can be found online at https://doi.org/10.1016/j.elecom.2025.108011. The Supplementary Information is available free of charge.

Supporting data for electrochemical characterization (geometrical current density as well as area-specific activity during the LSV protocol), dissolution study of the catalyst materials investigated in this study in the presence of metallic impurities

Data availability

Data will be made available on request.

References

[1] Lena V. Bühre, Mustafa Mourali, Patrick Trinke, Jonathan Brandt, Debora Brinker, Gözde Kardeş, André Weber, Boris Bensmann, Richard Hanke-Rauschenbach, Analysis of kinetic and ohmic resistances in PEM water electrolysis through reference electrode measurements, J. Electrochem. Soc. 171 (5) (2024) 054518.

[2] Christoph Immerz, Martin Schweins, Patrick Trinke, Boris Bensmann, Martin Paidar, Tomas Bystroň, Karel Bouzek, Richard Hanke-Rauschenbach, Experimental characterization of inhomogeneity in current density and temperature distribution along a single-channel PEM water electrolysis cell, Electrochim. Acta 260 (2018) 582–588.

[3] S.A. Grigoriev, K.A. Dzhus, D.G. Bessarabov, P. Millet, Failure of PEM water electrolysis cells: Case study involving anode dissolution and membrane thinning, Int. J. Hydrog. Energy 39 (35) (2014) 20440–20446.

[4] Heli Wang, John A. Turner, The influence of metal ions on the conductivity of Nafion 112 in polymer electrolyte membrane fuel cell, J. Power Sources 183 (2) (2008) 576–580.

[5] Michael J. Kelly, Günter Fafilek, Jürgen O. Besenhard, Hermann Kronberger, Gerhard E. Nauer, Contaminant absorption and conductivity in polymer electrolyte membranes, J. Power Sources 145 (2) (2005) 249–252.

[6] Xunying Wang, Linsong Zhang, Guangfu Li, Geng Zhang, Zhi-Gang Shao, Baolian Yi, The influence of ferric ion contamination on the solid polymer electrolyte water electrolysis performance, Electrochim. Acta 158 (2015) 253–257.

[7] Nuria Rojas, Margarita Sánchez-Molina, Gema Sevilla, Ernesto Amores, Eluxka Almandoz, Joseba Esparza, Marlon R. Cruz Vivas, Carles Colominas, Coated stainless steels evaluation for bipolar plates in PEM water electrolysis conditions, Int. J. Hydrog. Energy 46 (51) (2021) 25929–25943.

[8] Sasawat Mahabunphachai, Ömer Necati Cora, Muammer Koç, Effect of manufacturing processes on formability and surface topography of proton exchange membrane fuel cell metallic bipolar plates, J. Power Sources 195 (16) (2010) 5269–5277.
[9] Lena Fiedler, Tien-Ching Ma, Birk Fritsch, Jan H. Risse, Michael Lechner, Dominik Dworschak, Marion Merklein, Karl J.J. Mayrhofer, Andreas Hutzler, Stability of bipolar plate materials for proton-exchange membrane water electrolyzers: Dissolution of titanium and stainless steel in DI water and highly diluted acid, ChemElectroChem 10 (20) (2023) e202300373.
[10] Aldo Saul Gago, Asif Syed Ansar, Bilge Saruhan, Uwe Schulz, Philipp Lettenmeier, Natalia A. Cañas, Pawel Gazdzicki, Tobias Morawietz, Renate Hiesgen, Johannes Arnold, K. Andreas Friedrich, Protective coatings on stainless steel bipolar plates for proton exchange membrane (PEM) electrolysers, J. Power Sources 307 (2016) 815–825.
[11] Philipp Lettenmeier, Rainey Wang, Rami Abouatallah, Fabian Burggraf, Aldo Saul Gago, K. Andreas Friedrich, Coated stainless steel bipolar plates for proton exchange membrane electrolyzers, J. Electrochem. Soc. 163 (11) (2016) F3119.
[12] Na Li, Samuel Simon Araya, Søren Knudsen Kær, Long-term contamination effect of iron ions on cell performance degradation of proton exchange membrane water electrolyser, J. Power Sources 434 (2019) 226755.
[13] Na Li, Samuel Simon Araya, Søren Knudsen Kær, The effect of Fe3+ contamination in feed water on proton exchange membrane electrolyzer performance, Int. J. Hydrog. Energy 44 (26) (2019) 12952–12957.
[14] Linsong Zhang, Xiao Jie, Zhi-Gang Shao, Zhi-Min Zhou, Gang Xiao, Baolian Yi, The influence of sodium ion on the solid polymer electrolyte water electrolysis, Int. J. Hydrog. Energy 37 (2) (2012) 1321–1325.
[15] Na Li, Samuel Simon Araya, Xiaoti Cui, Søren Knudsen Kær, The effects of cationic impurities on the performance of proton exchange membrane water electrolyzer, J. Power Sources 473 (2020) 228617.
[16] Ana María Barrios Jiménez, Olga Sichevych, Ioannis Spanos, Simone G. Altendorf, Alim Ormeci, Iryna Antonyshyn, Al–Pt compounds catalyzing the oxygen evolution reaction, Dalton Trans 52 (5) (2023) 1433–1440.
[17] Muralidhar G. Chourashiya, Atsushi Urakawa, Solution combustion synthesis of highly dispersible and dispersed iridium oxide as an anode catalyst in PEM water electrolysis, J. Mater. Chem. A 5 (10) (2017) 4774–4778.
[18] Kangjae Lee, Jaehyuk Shim, Ho Yeon Jang, Hyeon Seok Lee, Heejong Shin, Byoung-Hoon Lee, Megalamane S. Bootharaju, Kug-Seung Lee, Jongmin Lee, Seongbeom Lee, Young-Hoon Lee, Chan Woo Lee, Yoon Jung, Guocheng Deng, Seungwoo Yoo, Seoin Back, Yung-Eun Sung, Taeghwan Hyeon, Modulating the valence electronic structure using earth-abundant aluminum for high-performance acidic oxygen evolution reaction, Chem 9 (12) (2023) 3600–3612.
[19] Qi Feng, Xiao-Zi Yuan, Gaoyang Liu, Bing Wei, Zhen Zhang, Hui Li, Haijiang Wang, A review of proton exchange membrane water electrolysis on degradation mechanisms and mitigation strategies, J. Power Sources 366 (2017) 33–55.
[20] Serhiy Cherevko, Simon Geiger, Olga Kasian, Andrea Mingers, Karl J.J. Mayrhofer, Oxygen evolution activity and stability of iridium in acidic media. Part 2. – Electrochemically grown hydrous iridium oxide, J. Electroanal. Chem. 774 (2016) 102–110.
[21] Serhiy Cherevko, Simon Geiger, Olga Kasian, Andrea Mingers, Karl J.J. Mayrhofer, Oxygen evolution activity and stability of iridium in acidic media. Part 1. – Metallic iridium, J. Electroanal. Chem. 773 (2016) 69–78.
[22] Jing Qi, Xiaofeng Wang, Ugur Pasaogullari, Leonard Bonville, Trent Molter, Effect of Al3+ contaminant on polymer electrolyte fuel cell performance, J. Electrochem. Soc. 160 (9) (2013) F916.
[23] Miklós Márton Kovács, Birk Fritsch, Leopold Lahn, Julien Bachmann, Olga Kasian, Karl J.J. Mayrhofer, Andreas Hutzler, Dominik Dworschak, Electrospun iridium-based nanofiber catalysts for oxygen evolution reaction: Influence of calcination on activity–stability relation, ACS Appl. Mater. & Interfaces 16 (39) (2024) 52179–52190.
[24] Sebastian O. Klemm, Angel A. Topalov, Claudius A. Laska, Karl J.J. Mayrhofer, Coupling of a high throughput microelectrochemical cell with online multi-elemental trace analysis by ICP-MS, Electrochem. Commun. 13 (12) (2011) 1533–1535.
[25] Simon Geiger, Olga Kasian, Marc Ledendecker, Enrico Pizzutilo, Andrea M. Mingers, Wen Tian Fu, Oscar Diaz-Morales, Zhizhong Li, Tobias Oellers, Luc Fruchter, Alfred Ludwig, Karl J.J. Mayrhofer, Marc T.M. Koper, Serhiy Cherevko, The stability number as a metric for electrocatalyst stability benchmarking, Nat. Catal. 1 (7) (2018) 508–515.
[26] Hans Becker, James Murawski, Dipak V. Shinde, Ifan E.L. Stephens, Gareth Hinds, Graham Smith, Impact of impurities on water electrolysis: a review, Sustain. Energy Fuels 7 (7) (2023) 1565–1603.
[27] Françoise Andolfatto, Robert Durand, Athanase Michas, Pierre Millet, Philippe S. Stevens, Solid polymer electrolyte water electrolysis: electrocatalysis and long-term stability, Int. J. Hydrog. Energy 19 (5) (1994) 421–427.
[28] Olga Kasian, Jan-Philipp Grote, Simon Geiger, Serhiy Cherevko, Karl J.J. Mayrhofer, The common intermediates of oxygen evolution and dissolution reactions during water electrolysis on iridium, Angew. Chem. Int. Ed. 57 (9) (2018) 2488–2491.
[29] Elliot Padgett, Anthony Adesso, Haoran Yu, Jacob Wrubel, Guido Bender, Bryan Pivovar, Shaun M. Alia, Performance losses and current-driven recovery from cation contaminants in PEM water electrolysis, J. Electrochem. Soc. 171 (6) (2024) 064510.
[30] Steffen Henrik Frensch, Guillaume Serre, Frédéric Fouda-Onana, Henriette Casper Jensen, Morten Lykkegaard Christensen, Samuel Simon Araya, Søren Knudsen Kær, Impact of iron and hydrogen peroxide on membrane degradation for polymer electrolyte membrane water electrolysis: Computational and experimental investigation on fluoride emission, J. Power Sources 420 (2019) 54–62.
[31] Kitiya Hongsirikarn, James G. Goodwin, Scott Greenway, Stephen Creager, Effect of cations (Na+, Ca2+, Fe3+) on the conductivity of a Nafion membrane, J. Power Sources 195 (21) (2010) 7213–7220.
[32] Tatsuhiro Okada, Yuusuke Ayato, Makoto Yuasa, Isao Sekine, The effect of impurity cations on the transport characteristics of perfluorosulfonated ionomer membranes, J. Phys. Chem. B 103 (17) (1999) 3315–3322.
[33] Linsong Zhang, Xiao Jie, Zhi-Gang Shao, Xunying Wang, Baolian Yi, The dynamic-state effects of sodium ion contamination on the solid polymer electrolyte water electrolysis, J. Power Sources 241 (2013) 341–348.
[34] Tatsuhiro Okada, Norito Nakamura, Makoto Yuasa, Isao Sekine, Ion and water transport characteristics in membranes for polymer electrolyte fuel cells containing H+ and Ca2+ cations, J. Electrochem. Soc. 144 (8) (1997) 2744.
[35] Tatsuhiro Okada, Steffen Møller-Holst, Oddvar Gorseth, Signe Kjelstrup, Transport and equilibrium properties of Nafion® membranes with H+ and Na+ ions, J. Electroanal. Chem. 442 (1) (1998) 137–145.
[36] Shouwen Shi, Adam Z. Weber, Ahmet Kusoglu, Structure-transport relationship of perfluorosulfonic-acid membranes in different cationic forms, Electrochim. Acta 220 (2016) 517–528.
[37] Shucheng Sun, Zhigang Shao, Hongmei Yu, Guangfu Li, Baolian Yi, Investigations on degradation of the long-term proton exchange membrane water electrolysis stack, J. Power Sources 267 (2014) 515–520.
[38] Jingke Mo, Stuart Steen, Zhenye Kang, Gaoqiang Yang, Derrick A. Taylor, Yifan Li, Todd J. Toops, Michael P. Brady, Scott T. Retterer, David A. Cullen, Johney B. Green, Feng-Yuan Zhang, Study on corrosion migrations within catalyst-coated membranes of proton exchange membrane electrolyzer cells, Int. J. Hydrog. Energy 42 (44) (2017) 27343–27349.
[39] Ugljesa Babic, Mateusz Zlobinski, Thomas Justus Schmidt, Pierre Boillat, Lorenz Gubler, CO2-assisted regeneration of a polymer electrolyte water electrolyzer contaminated with metal ion impurities, J. Electrochem. Soc. 166 (10) (2019) F610.
[40] Aidong Tan, Yipeng Zhang, Xiaoyun Shi, Chen Ju, Ping Liu, Tianrang Yang, Jianguo Liu, The poisoning effects of Ti-ion from porous transport layers on the membrane electrode assembly of proton exchange membrane water electrolyzers, Chem. Eng. J. 471 (2023) 144624.
[41] Michael J. Kelly, Bernhard Egger, Günter Fafilek, Jürgen O. Besenhard, Hermann Kronberger, Gerhard E. Nauer, Conductivity of polymer electrolyte membranes by impedance spectroscopy with microelectrodes, Solid State Ion. 176 (25) (2005) 2111–2114.
[42] PyaePyae Shwe Sin, SoeHtet Wai, Yasuyuki Ota, Kensuke Nishioka, Yoshihiro Suzuki, Performance recovery of proton exchange membrane electrolyzer degraded by metal cations contamination, Int. J. Hydrog. Energy 53 (2024) 86–92.
[43] Alberto Ganassin, Viktor Colic, Jakub Tymoczko, Aliaksandr S. Bandarenka, Wolfgang Schuhmann, Non-covalent interactions in water electrolysis: influence on the activity of Pt(111) and iridium oxide catalysts in acidic media, Phys. Chem. Chem. Phys. 17 (13) (2015) 8349–8355.
[44] Johannes G. Vos, Zhichao Liu, Florian D. Speck, Nickson Perini, Wentian Fu, Serhiy Cherevko, Marc T.M. Koper, Selectivity trends between oxygen evolution and chlorine evolution on iridium-based double perovskites in acidic media, ACS Catal. 9 (9) (2019) 8561–8574.